Shape Optimization of One-chamber Mufflers with Perforated Intruding Tubes Using a Simulated Annealing Method

Min-Chie Chiu[1]、Ying-Chun Chang[2]、Wang-Chuan Liu[3]

Abstract

It has been noted that the application of high performance, compact mufflers is the future for modern factories where place is at a premium. However, as research on mufflers equipped with extended tubes has been exhausted, and frankly at the juncture, shown to be inadequate (unsuitable), attention has turn to mufflers conjugated with perforated intruding tubes which can dramatically increase acoustical performance. Therefore, the focus of this paper is not only to analyze the sound transmission loss (*STL*) of a one-chamber open-ended perforated muffler but also to optimize the best design shape within a limited space.

In this paper, the four-pole system matrix for evaluating the acoustic performance — sound transmission loss (*STL*) — is derived by using a decoupled numerical method. Additionally, a simulated annealing (*SA*), a robust scheme used to search for the global optimum by imitating the metal's heating process, has been used during the optimization process. Before dealing with a broadband noise, the *STL*'s maximization with respect to a one-tone noise is introduced for a reliability check on the *SA* method. Also, an accuracy check on the mathematical model is performed. To appreciate the acoustical ability of the new mufflers, traditional mufflers, including a simple expansion muffler as well as a non-perforated intruding-tube muffler, have been assessed. Results reveal that the maximal *STL* is precisely located at the desired targeted tone. In addition, the acoustical performance of mufflers conjugated with perforated intruding tubes is found to be superior to the traditional mufflers. Consequently, the approach used for the optimal design of the noise elimination proposed in this study is quite effective.

Keywords: perforated intruding tube、decoupled numerical method、space constraints、simulated annealing

[1] Assistant Professor, Department of Automatic Control Engineering, Chungchou Institute of Technology
[2] Associate Professor, Department of Mechanical Engineering, Tatung University
[3] Graduate Student, Department of Mechanical Engineering, Tatung University

1. Introduction

To overcome the low frequency noise emitted from venting systems, mufflers have been continually used [1]. Research on mufflers was started by Davis *et al.* in 1954 [2]. Based on the plane wave theory, studies of simple expansion mufflers without perforated holes have been made [3, 4, 5]. To increase a muffler's acoustical performance, the assessment of a new acoustical element — internal perforated plug tubes — was discussed by Sullivan and Crocker [6]. On the basis of the coupled differential equations, a series of theoretical and numerical techniques in decoupling the acoustical problems have been proposed [7, 8, 9, 10]. In 1981, Jayaraman and Yam [11] developed a method in finding an analytical solution; however, a presumption of the velocity equality within the inner and outer duct, which is not reasonable in the real world, is required. To overcome this drawback, Munjal *et al*. [12] provided a generalized de-coupling method. Regarding the flowing effect, Peat [13] publicized the numerical decoupling method by finding the eigen value in transfer matrices.

In order to maintain a steady volume-flow-rate in a venting system, a muffler's back pressure within an allowable range is compulsory. Therefore, Wang [14] developed a perforated intruding-tube muffler (a low back-pressure muffler with non-plug tubes inside the cavity) using BEM (Boundary Element Method). However, the need to investigate the optimal muffler design within certain space constraints is rarely seen. In previous work [15, 16, 17, 18], the shape optimization of a low back-pressure muffler (a one-chamber simple expansion muffler and a one-chamber conjugated muffler with non-perforated intruding tubes) using a GA (genetic algorithm) and gradient methods within a space-constrained situation has been addressed; yet, the acoustical performance of above mufflers is still insufficient. In order to efficiently improve the performance of the noise control device and maintain a steady volume-flow-rate within a space-constrained situation, an optimal design on a one-chamber muffler equipped with perforated intruding tubes is presented. In this paper, the four-pole system matrix for evaluating the acoustic performance — sound transmission loss (*STL*) — is derived by using a decoupled numerical method. A *SA* method patterned after the Darwinian notion of natural selection is applied in this work.

3. Theoretical Background

In this paper, a one-chamber muffler with perforated intruding tubes was adopted for noise elimination in the fan room shown in Figure 1. Before the acoustical fields of the mufflers are analyzed, the acoustical elements have been distinguished. As shown in Figure 2, three kinds of muffler components, including three straight tubes, a perforated intruding inlet tube, and a perforated intruding outlet tube, are identified and symbolized as I, II, and III. In addition, the acoustic pressure $\overline{p}$ and acoustic particle velocity $\overline{u}$ within the muffler are depicted in Figure 3 where the acoustical field is represented by six points.

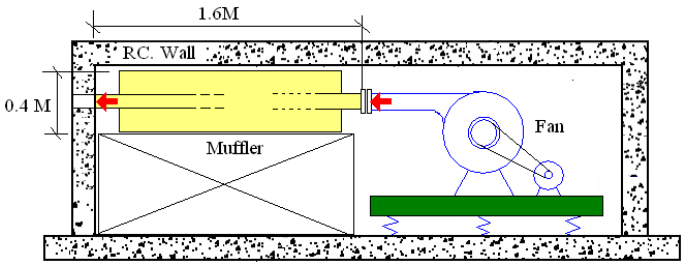

Figure 1　Noise elimination of a fan noise inside a limited space.

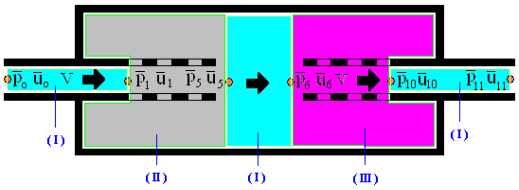

Figure 2　Acoustical elements in a one-chamber muffler hybridized with perforated intruding tubes.

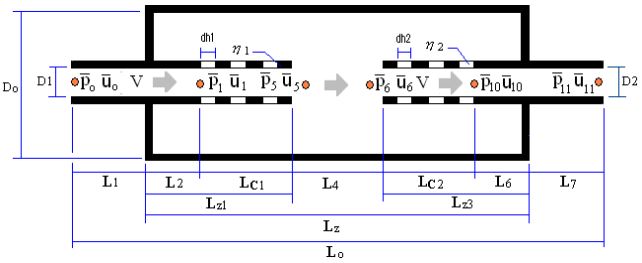

Figure 3　The outline dimension and acoustical field in a one-chamber muffler hybridized with perforated intruding tubes.

The muffler system is composed of three kinds of acoustical elements. The individual transfer matrix derivations with respect to three kinds of acoustical mechanisms are described as below.

3.1 Transfer Matrix for a Straight Tube

For a one dimensional wave propagating in a symmetric straight tube shown in Figure 3, the acoustic pressure and particle velocity are

$$p(x,t) = \left(k_1 e^{-jkx/(1+M)} + k_2 e^{+jkx/(1-M)}\right) e^{jwt} \tag{1}$$

$$u(x,t) = \left(\frac{k_1}{\rho_o c_o} e^{-jkx/(1+M)} - \frac{k_2}{\rho_o c_o} e^{+jkx/(1-M)}\right) e^{jwt} \tag{2}$$

Considering boundary conditions of pt 0 (x=0) and pt 1 (x=L), Eqs. (1) and (2) can be rearranged as

$$\begin{pmatrix} p_o(0,0) \\ \rho_o c_o u_o(0,0) \end{pmatrix} = \begin{bmatrix} 1 & 1 \\ 1 & -1 \end{bmatrix} \begin{pmatrix} k_1 \\ k_2 \end{pmatrix} \tag{3}$$

$$\begin{pmatrix} p_1(L,0) \\ \rho_o c_o u_1(L,0) \end{pmatrix} = \begin{bmatrix} e^{-jk^+L} & e^{+jk^-L} \\ e^{-jk^+L} & -e^{+jk^-L} \end{bmatrix} \begin{pmatrix} k_1 \\ k_2 \end{pmatrix} \tag{4}$$

A combination of Eqs. (3) and (4) yields

$$\begin{pmatrix} \bar{p}_o \\ \rho_o c_o \bar{u}_o \end{pmatrix} = e^{-j\frac{M_1 k(L_1+L_2)}{1-M_1^2}} \begin{bmatrix} TS1_{1,1} & TS1_{1,2} \\ TS1_{2,1} & TS1_{2,2} \end{bmatrix} \begin{pmatrix} \bar{p}_1 \\ \rho_o c_o \bar{u}_1 \end{pmatrix} \tag{5}$$

Similarly, the transfer matrix between pt 5 and pt 6 is

$$\begin{pmatrix} \bar{p}_5 \\ \rho_o c_o \bar{u}_5 \end{pmatrix} = e^{-j\frac{M_5 k L_4}{1-M_5^2}} \begin{bmatrix} TS2_{1,1} & TS2_{1,2} \\ TS2_{2,1} & TS2_{2,2} \end{bmatrix} \begin{pmatrix} \bar{p}_6 \\ \rho_o c_o \bar{u}_6 \end{pmatrix} \tag{6}$$

Likewise, the transfer matrix between pt 10 and pt 11 is

$$\begin{pmatrix} \bar{p}_{10} \\ \rho_o c_o \bar{u}_{10} \end{pmatrix} = e^{-j\frac{M_{10} k(L_6+L_7)}{1-M_{10}^2}} \begin{bmatrix} TS3_{1,1} & TS3_{1,2} \\ TS3_{2,1} & TS3_{2,2} \end{bmatrix} \begin{pmatrix} \bar{p}_{11} \\ \rho_o c_o \bar{u}_{11} \end{pmatrix} \tag{7}$$

3.2 Transfer Matrix of a Perforated Intruding Inlet Tube

To analysis the acoustical mechanism of element (II), a detailed acoustical field represented by five points is depicted in Figure 4. Based on Sullivan and Crocker's derivation [6], the continuity equations and momentum equations with respect to inner and outer tubes at nodes 1 and 2 are as follows.

Inner tube:

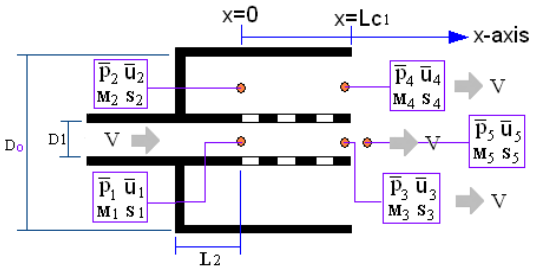

Figure 4 The acoustical mechanism of a perforated intruding inlet tubes.

continuity equation

$$V_1 \frac{\partial \rho_1}{\partial x} + \rho_o \frac{\partial u_1}{\partial x} + \frac{4\rho_o}{D_1} u + \frac{\partial \rho_2}{\partial t} = 0 \tag{8}$$

momentum equation:

$$\rho_o \left(\frac{\partial}{\partial t} + V_1 \frac{\partial}{\partial x} \right) u_1 + \frac{\partial p_1}{\partial x} = 0 \tag{9}$$

Outer tube:

continuity equation

$$\rho_o \frac{\partial u_2}{\partial x} - \frac{4 D_2 \rho_o}{D_O^2 - D_1^2} u + \frac{\partial \rho_2}{\partial t} = 0 \tag{10}$$

$$\rho_o\left(\frac{\partial}{\partial t}+V_2\frac{\partial}{\partial x}\right)u_2+\frac{\partial p_2}{\partial x}=0 \tag{11}$$

Assuming that the acoustic wave is a harmonic motion

$$p(x,t)=P(x)\cdot e^{j\omega t} \tag{12}$$

Under the isentropic processes in ducts, it has

$$P(x)=\rho(x)\cdot c_o^2 \tag{13}$$

Assuming that the perforation along the inner tube is uniform (ie. $d\varsigma/dx=0$), the acoustic impedance of the perforation ($\rho_o\, c_o\, \varsigma$) is

$$\rho_o\, c_o\, \varsigma=\frac{p_1(x)-p_2(x)}{u(x)} \tag{14}$$

where ς is the specific acoustical impedance of the perforated tube. According to the experience formula of ς developed by Sullivan [6] and Rao [10], the empirical formulations for the perforate tube with and without mean flow have been adopted in this study.

By substituting Eqs.(12)~(14) into Eqs. (8)~(11), we have

$$\left\{\frac{d^2}{dx^2}-\frac{jM_1}{1-M_1^2}\left[\frac{k_a^2+k^2}{k}\right]\frac{d}{dx}+\frac{k_a^2}{1-M_1^2}\right\}p_1=-\left\{\frac{jM_1}{1-M_1^2}\left[\frac{k_a^2-k^2}{k}\right]\frac{d}{dx}-\frac{k_a^2-k^2}{1-M_1^2}\right\}p_2 \tag{15a}$$

$$\rho_o\left(\frac{\partial}{\partial t}+V_1\frac{\partial}{\partial x}\right)u_1+\frac{\partial}{\partial x}p_1=0 \tag{15b}$$

$$\left\{\frac{d^2}{dx^2}-\frac{jM_2}{1-M_2^2}\left[\frac{k_b^2+k^2}{k}\right]\frac{d}{dx}+\frac{k_a^2}{1-M_2^2}\right\}p_2=-\left\{\frac{jM_2}{1-M_2^2}\left[\frac{k_b^2-k^2}{k}\right]\frac{d}{dx}-\frac{k_b^2-k^2}{1-M_2^2}\right\}p_1 \tag{15c}$$

$$\rho_o\left(\frac{\partial}{\partial t}+V_2\frac{\partial}{\partial x}\right)u_2+\frac{\partial}{\partial x}p_2=0 \tag{15d}$$

Eliminating u_1 and u_2 by the differentiation and substitution of Eq.(15) yields

$$\begin{bmatrix} D^2+\alpha_1 D+\alpha_2 & \alpha_3 D+\alpha_4 \\ \alpha_5 D+\alpha_6 & D^2+\alpha_7 D+\alpha_8 \end{bmatrix}\begin{bmatrix} p_1 \\ p_2 \end{bmatrix}=\begin{bmatrix} 0 \\ 0 \end{bmatrix} \tag{16a}$$

Developing Eq.(16a), we obtain

$$p_1''+\alpha_1 p_1'+\alpha_2 p_1+\alpha_3 p_2'+\alpha_4 p_2=0 \tag{17a}$$

$$\alpha_5 p_1'+\alpha_6 p_1+p_2''+\alpha_7 p_2'+\alpha_8 p_2=0 \tag{17b}$$

$$\text{Let}\quad p_1'=\frac{dp_1}{dx}=y_1,\quad p_2'=\frac{dp_2}{dx}=y_2,\quad p_1=y_3,\quad p_2=y_4 \tag{18}$$

According to Eqs. (17) and (18), the new matrix between {y'} and {y} is

$$\begin{bmatrix} y_1' \\ y_2' \\ y_3' \\ y_4' \end{bmatrix} = \begin{bmatrix} -\alpha_1 & -\alpha_3 & -\alpha_2 & -\alpha_4 \\ -\alpha_5 & -\alpha_7 & -\alpha_6 & -\alpha_8 \\ 1 & 0 & 0 & 0 \\ 0 & 1 & 0 & 0 \end{bmatrix} \begin{bmatrix} y_1 \\ y_2 \\ y_3 \\ y_4 \end{bmatrix} \tag{19a}$$

which can be briefly expressed as

$$\{y'\} = [\mathrm{N}]\{y\} \tag{19b}$$

Let $\{y\} = [\Omega]\{\Gamma\}$ (20a)

which is

$$\begin{bmatrix} dp_1/dx \\ dp_2/dx \\ p_1 \\ p_2 \end{bmatrix} = \begin{bmatrix} \Omega_{1,1} & \Omega_{1,2} & \Omega_{1,3} & \Omega_{1,4} \\ \Omega_{2,1} & \Omega_{2,2} & \Omega_{2,3} & \Omega_{2,4} \\ \Omega_{3,1} & \Omega_{3,2} & \Omega_{3,3} & \Omega_{3,4} \\ \Omega_{4,1} & \Omega_{4,2} & \Omega_{4,3} & \Omega_{4,4} \end{bmatrix} \begin{bmatrix} \Gamma_1 \\ \Gamma_2 \\ \Gamma_3 \\ \Gamma_4 \end{bmatrix} \tag{20b}$$

$[\Omega]_{4x4}$ is the model matrix formed by four sets of eigen vectors Ω_{4x1} of $[\mathrm{N}]_{4x4}$.

Substituting Eq.(21) into (20)and then multiplying $[\Omega]^{-1}$ by both sides yields

$$[\Omega]^{-1}[\Omega]\{\Gamma'\} = [\Omega]^{-1}[\mathrm{N}][\Omega]\{\Gamma\} \tag{21}$$

Set $[\chi] = [\Omega]^{-1}[\mathrm{N}][\Omega] = \begin{bmatrix} \beta_1 & 0 & 0 & 0 \\ 0 & \beta_2 & 0 & 0 \\ 0 & 0 & \beta_3 & 0 \\ 0 & 0 & 0 & \beta_4 \end{bmatrix}$ (22)

Eq.(20) can be thus rewritten as

$$\{\Gamma'\} = [\chi]\{\Gamma\} \tag{23}$$

Obviously, Eq.(23) is a decoupled equation. The related solution can then be written as

$$\Gamma_i = C_i e^{\beta_i x} \tag{24}$$

Using Eqs.(9),(11),(20) and (24), the relationship of acoustic pressure and particle velocity is

$$\begin{bmatrix} p_1(x) \\ p_2(x) \\ \rho_o c_o u_1(x) \\ \rho_o c_o u_2(x) \end{bmatrix} = \begin{bmatrix} \mathrm{H}_{1,1} & \mathrm{H}_{1,2} & \mathrm{H}_{1,3} & \mathrm{H}_{1,4} \\ \mathrm{H}_{2,1} & \mathrm{H}_{2,2} & \mathrm{H}_{2,3} & \mathrm{H}_{2,4} \\ \mathrm{H}_{3,1} & \mathrm{H}_{3,2} & \mathrm{H}_{3,3} & \mathrm{H}_{3,4} \\ \mathrm{H}_{4,1} & \mathrm{H}_{4,2} & \mathrm{H}_{4,3} & \mathrm{H}_{4,4} \end{bmatrix} \begin{bmatrix} k_1 \\ k_2 \\ k_3 \\ k_4 \end{bmatrix} \tag{25}$$

Substituting x=0 and x=Lc$_1$ into Eq.(25) and doing rearrangement yield

$$\begin{bmatrix} p_1(0) \\ p_2(0) \\ \rho_o c_o u_1(0) \\ \rho_o c_o u_2(0) \end{bmatrix} = [\mathrm{T}] \begin{bmatrix} p_1(L_C) \\ p_2(L_C) \\ \rho_o c_o u_1(L_C) \\ \rho_o c_o u_2(L_C) \end{bmatrix} \tag{26}$$

Eq.(26) can be represented by the new symbols $\overline{p}_1, \overline{p}_2, \overline{p}_3, \overline{p}_4, \overline{u}_1, \overline{u}_2, \overline{u}_3$ and $\overline{u}_4$

$$\begin{bmatrix} \overline{p}_1 \\ \overline{p}_2 \\ \rho_o c_o \overline{u}_1 \\ \rho_o c_o \overline{u}_2 \end{bmatrix} = [\mathrm{T}] \begin{bmatrix} \overline{p}_3 \\ \overline{p}_4 \\ \rho_o c_o \overline{u}_3 \\ \rho_o c_o \overline{u}_4 \end{bmatrix} \tag{27}$$

The equation of mass continuity between point 3 and point 5 with mean flow is expressed in equation (28)

$$\begin{aligned} & c_o \rho_o S_3 \overline{u}_3 + S_3 M_3 \overline{p}_3 \\ & = c_o \rho_o S_5 \overline{u}_5 + c_o \rho_o S_4 \overline{u}_4 + S_5 M_5 \left(\overline{p}_5 - \frac{p_o}{C_v} \frac{R K_e M_5 Y_5}{p_o} \frac{v_{c,5} - M_5 p_{c,5} / Y_5}{1 - M_5^{\,2}} \right) \end{aligned} \tag{28a}$$

or

$$\begin{aligned} & c_o \rho_o S_3 \overline{u}_3 + S_3 M_3 \overline{p}_3 \\ & = c_o \rho_o S_5 \overline{u}_5 + c_o \rho_o S_4 \overline{u}_4 + S_5 M_5 \left(\overline{p}_5 - \frac{p_o (\gamma - 1) K_e M_5 Y_5}{p_o} \frac{v_{c,5} - M_5 p_{c,5} / Y_5}{1 - M_5^{\,2}} \right) \end{aligned} \tag{28b}$$

A concept of static enthalpy deduced by Munjal [19] is described as

$$\begin{bmatrix} p_{c,5} \\ v_{c,5} \end{bmatrix} = \begin{bmatrix} 1 & M_5 Y_5 \\ \dfrac{M_5}{Y_5} & 1 \end{bmatrix} \begin{bmatrix} \overline{p}_5 \\ \rho_o S_5 \overline{u}_5 \end{bmatrix} \tag{29}$$

Substituting Eq. (29) into Eq. (28), we have

$$\begin{aligned} & c_o \rho_o S_3 \overline{u}_3 + S_3 M_3 \overline{p}_3 \\ & = c_o \rho_o S_5 \overline{u}_5 \left[1 - \frac{(\gamma - 1)}{c_o} Y_5 K_e S_5 M_5^2 \right] + \left(M_5 S_5 \overline{p}_5 + c_o \rho_o \overline{u}_4 S_4 \right) \end{aligned} \tag{30}$$

The equation of momentum for steady flow is

$$\begin{aligned} & S_3 \left(1 + M_3^2 \right) \overline{p}_3 + 2 \rho_o c_o S_3 M_3 \overline{u}_3 + c_{11} \left(S_5 + S_5 M_5^2 \right) \overline{p}_5 \\ & = -c_{11} \left(\frac{2 S_5}{c_o} - \frac{(\gamma - 1) K_e M_5^3 Y_5 S_5^2}{c_o} \right) \rho_o c_o \overline{u}_5 - c_{12} S_4 \overline{p}_4 \end{aligned} \tag{31}$$

The equation of energy conservation for steady flow is

$$\overline{p}_3 + \rho_o V_3 \overline{u}_3 = \overline{p}_5 + \rho_o V_5 \overline{u}_5 + K_e \rho_o V_5 \overline{u}_5 \tag{32}$$

With the rigid wall at boundary, we have

$$\frac{\overline{p}_2}{\rho_o c_o \overline{u}_2} = -j \cot(k L_2) \tag{33}$$

By substituting and eliminating parameters $\overline{p}_2, \overline{u}_2$, $\overline{p}_3, \overline{u}_3, \overline{p}_4, \overline{u}_4$, the simplified equations become

$$\bar{p}_1 = \frac{N_3N_6 - N_7N_2}{N_1N_6 - N_5N_2}\bar{p}_5 + \frac{N_4N_6 - N_8N_2}{N_1N_6 - N_5N_2}\rho_o c_o \bar{u}_5 \tag{34a}$$

$$\rho_o c_o \bar{u}_1 = -\frac{N_3N_5 - N_7N_1}{N_1N_6 - N_5N_2}\bar{p}_5 - \frac{N_4N_5 - N_8N_1}{N_1N_6 - N_5N_2}\rho_o c_o \bar{u}_5 \tag{34b}$$

Combining Eqs(34a,b) into a matrix form yields

$$\begin{bmatrix} \bar{p}_1 \\ \rho_o c_o \bar{u}_1 \end{bmatrix} = \begin{bmatrix} TPOE_{1,1} & TPOE_{1,2} \\ TPOE_{2,1} & TPOE_{2,2} \end{bmatrix} \begin{bmatrix} \bar{p}_5 \\ \rho_o c_o \bar{u}_5 \end{bmatrix} \tag{35}$$

3.3 Transfer Matrix of a Perforated Intruding Outlet Tube

Similarly, for a perforated intruding tube shown in Figure 5, its geometry is symmetrical to the above perforated intruding outlet tube. As derived in Eqs. (8)~(35), the acoustical pressure and acoustical particle velocity at points 7 and 8 is

$$\bar{p}_7 = (TT_{1,1}\bar{p}_9 + TT_{1,3}X)\bar{p}_9 + TT_{1,2}\bar{p}_{10} + TT_{1,4}\rho_o c_o \bar{u}_{10} \tag{36a}$$

$$\bar{p}_8 = (TT_{2,1} + TT_{2,3}X)\bar{p}_9 + TT_{2,2}\bar{p}_{10} + TT_{2,4}\rho_o c_o \bar{u}_{10} \tag{36b}$$

$$\rho_o c_o \bar{u}_7 = (TT_{3,1} + TT_{3,3}X)\bar{p}_9 + TT_{3,2}\bar{p}_{10} + TT_{3,4}\rho_o c_o \bar{u}_{10} \tag{36c}$$

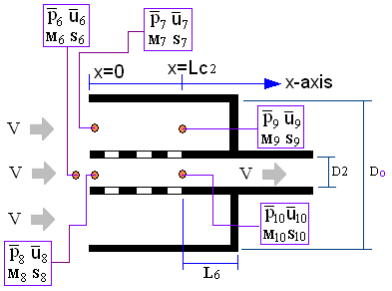

Figure 5 The acoustical mechanism of a perforated intruding outlet tube.

$$\rho_o c_o \bar{u}_8 = (TT_{4,1} + TT_{4,3}X)\bar{p}_9 + TT_{4,2}\bar{p}_{10} + TT_{4,4}\rho_o c_o \bar{u}_{10} \tag{36d}$$

By substituting and eliminating parameters ($\bar{p}_7, \bar{u}_7, \bar{p}_8, \bar{u}_8, \bar{p}_9, \bar{u}_9$) in Eq.(41), the simplified equations become

$$\bar{p}_6 = \frac{NN_7NN_2 - NN_3NN_6}{NN_5NN_2 - NN_1NN_6}\bar{p}_{10} + \frac{NN_8NN_2 - NN_4NN_6}{NN_5NN_2 - NN_1NN_6}\rho_o c_o \bar{u}_{10} \tag{37a}$$

$$\rho_o c_o \bar{u}_6 = \frac{NN_7NN_1 - NN_3NN_5}{NN_6NN_1 - NN_2NN_5}\bar{p}_{10} + \frac{NN_8NN_1 - NN_4NN_5}{NN_6NN_1 - NN_2NN_5}\rho_o c_o \bar{u}_{10} \tag{37b}$$

Combining Eqs(37a,b) into a matrix form yields

$$\begin{bmatrix} \overline{p}_6 \\ \rho_o c_o \overline{u}_6 \end{bmatrix} = \begin{bmatrix} TPOC_{1,1} & TPOC_{1,2} \\ TPOC_{2,1} & TPOC_{2,2} \end{bmatrix} \begin{bmatrix} \overline{p}_{10} \\ \rho_o c_o \overline{u}_{10} \end{bmatrix} \tag{38}$$

3.4 Sound Transmission Loss

For combining above Eqs., the total transfer matrix assembled by multiplication is

$$\begin{bmatrix} \overline{p}_o \\ \rho_o c_o \overline{u}_o \end{bmatrix} = \begin{bmatrix} T_{11}^* & T_{12}^* \\ T_{21}^* & T_{22}^* \end{bmatrix} \begin{pmatrix} \overline{p}_{11} \\ \rho_o c_o \overline{u}_{11} \end{pmatrix} \tag{39}$$

$$\begin{aligned} &STL\left(Q, f, RT_1, RT_2, RT_3, RT_4, RT_5, RT_6, RT_7, RT_8, RT_9, RT_{10}\right) \\ &= \log\left(\frac{\left|T_{11}^* + T_{12}^* + T_{21}^* + T_{22}^*\right|}{2}\right) + 10\log\left(\frac{S_1}{S_{11}}\right) \end{aligned} \tag{40}$$

3.5 Overall Sound Power Level

$$\begin{aligned} SWL_T &= 10 * \log\{\sum_{i=1}^{5} 10^{SWL_i/10}\} \\ &= 10 * \log\left\{\begin{matrix} 10^{[SWLO(f=125)-STL(f=125)]} + 10^{[SWLO(f=250)-STL(f=250)]/10} \\ + 10^{[SWLO(f=500)-STL(f=500)]/10} + 10^{[SWLO(f=1000)-STL(f=1000)]/10} + 10^{[SWLO(f=2000)-STL(f=2000)]/10} \end{matrix}\right\} \end{aligned} \tag{41}$$

3.6 Objective Function

By using the formulas of Eqs.(40)(41), the objective function used in the S*A* optimization was established.

(A) *STL* maximization for a one- tone (*f*) noise

$$OBJ_1 = \left(Q, f, RT_1, RT_2, RT_3, RT_4, RT_5, RT_6, RT_7, RT_8, RT_9, RT_{10}\right) \tag{42}$$

(B) *SWL* minimization for a broadband noise

To minimize the overall SWL_T, the objective function is

$$OBJ_2 = SWL_T\left(Q, f, RT_1, RT_2, RT_3, RT_4, RT_5, RT_6, RT_7, RT_8, RT_9, RT_{10}\right) \tag{43}$$

4. Model Check

Before performing the *SA* optimal simulation on mufflers, an accuracy check of the mathematical model on a one-chamber muffler with perforated intruding tubes is performed by Wang *et al.* [14]. As indicated in Figure 6, the accuracy comparisons between theoretical data and analytical data are in agreement. Therefore, the model of a one-chamber muffler with perforated intruding tubes is acceptable and adopted in the following optimization process.

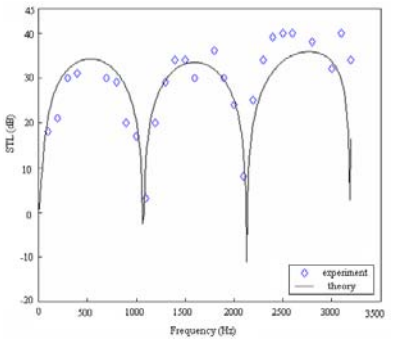

Figure 6 Performance of a one-chamber muffler equipped with perforated intruding tubes [Experimental data is from Wang *et al.* [14]].

5. Case Studies

In this paper, the noise reduction of a space-constrained fan room is exemplified and shown in Figure 1. The sound power level (*SWL*) inside the fan's outlet is shown in Table 1 where the overall *SWL* reaches 122.4 dB. To depress the huge venting noise emitted from the fan's outlet, a one-chamber muffler hybridized with perforated intruding tubes is considered. To obtain the best acoustical performance within a fixed space, numerical assessments linked to a *SA* optimizer are applied. Before the minimization of a broadband noise is executed, a reliability check of the *SA* method by maximization of the *STL* at a targeted one tone (250 Hz) has been carried out. As indicated in Figure 7, to appreciate the acoustic performance, two kinds of low back-pressure mufflers (one, a simple expansion muffler; and the other, a muffler hybridized with non-perforated intruding tubes) are accessed and optimized. As shown in Figures 1 and 2, the available space for a muffler is 0.4 m in width, 0.4 m in height, and 1.6 m in length. The flow rate (Q) and thickness of a perforated tube (t) are preset at 0.05 (m^3/s) and 0.001(m), respectively.

Table 1 Unsilenced *SWL* of a fan inside a duct outlet.

Frequency - Hz	125	250	500	1000	2000	4000
SWLO - dB	115	120	116	102	96	88

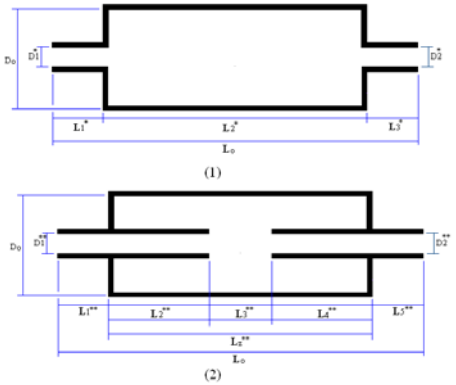

Figure 7 Two kinds of low back-pressure mufflers [(1) a one-chamber simple expansion muffler; (2) a one-chamber muffler hybridized with non-perforated intruding tubes].

6. Simulated Annealing Method

The basic concept behind simulated annealing (*SA*) was first introduced by Metropolis et al. [20] and developed by Kirkpatrick *et al.* [21]. The simulated annealing (*SA*) algorithm is a local search process which imitates the softening process (annealing) of metal. In the physical system, annealing is the process of heating and keeping a metal at a stabilized temperature while cooling it slowly. Slow cooling allows the particles to keep their state close to the minimal energy state. In this state, the particles have a more homogeneous crystalline structure. Conversely, a fast cooling rate results in a higher distorted energy that is stored inside the imperfect lattice.

The algorithm starts by generating a random initial solution. The scheme of SA is a variation of the hill-climbing algorithm. As indicated in Figure 8, all downhill movements for improvement are accepted for the decrement of the system's energy. Simultaneously, *SA* also allows movement resulting in solutions that are worse (uphill moves) than the current solution. This is done in order to escape from the local optimum.

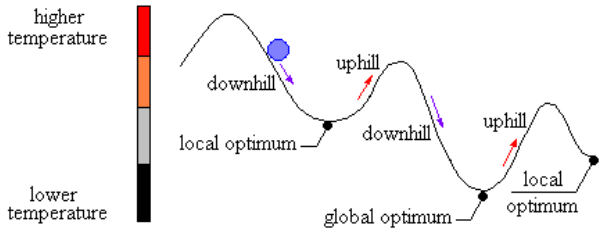

Figure 8 SA algorithm from a physical viewpoint.

As indicated in Figure 9, to imitate the evolution of the SA algorithm, a new random solution (*X'*) is chosen from the neighborhood of the current solution (*X*). If the change in the objective function (or energy) is negative, ie., $\Delta F \le 0$, a new solution will be acknowledged as the new current solution with the transition property *pb*(*X'*) of 1; if it is not negative, then the new transition property (*pb(X')*) varying from 0~1 will be calculated by the Boltzmann's factor (*pb(X')* = $\exp(\Delta F / CT)$) as shown in Eq. (44).

$$pb(X') = \begin{cases} 1, \Delta F \le 0 \\ \exp(\dfrac{-\Delta F}{CT}), \Delta f > 0 \end{cases} \quad (44a)$$

$$\Delta F = OBJ(X') - OBJ(X) \quad (44b)$$

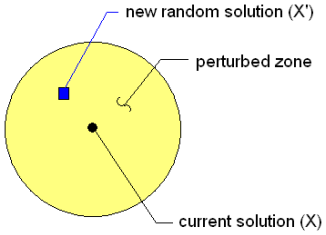

Figure 9 New random solution in a perturbed zone.

where the *C* and *T* are the Boltzmann constant and the current temperature. Additionally, compared to the new random probability of rand(0,1), if the transition property (*pb(X')*) is

greater than a random number of rand(0,1), the new uphill solution, which results in a higher energy condition, will then be accepted; otherwise, it is rejected. The uphill solution at a higher temperature will therefore have a better chance of escaping from the local optimum. The algorithm repeats the perturbation of the current solution and the measurement of the change in the objective function. As indicated in Figure 10, each successful substitution of the new current solution will lead to the decay of the current temperature as

$$T_{new} = kk * T_{old} \tag{45}$$

7. Results and Discussion

7.1 Results

To achieve good optimization, two kinds of *SA* parameters, including the cooling rate (*kk*) and the number of iterations (*Iter*) and (*pm*) are varied step by step during optimization. Two results of optimization (one, pure tone noises used for *SA*'s accuracy check; and the other, a broadband noise occurring in a fan room) are described below.

7.1.1 Pure Tone Noise Optimization

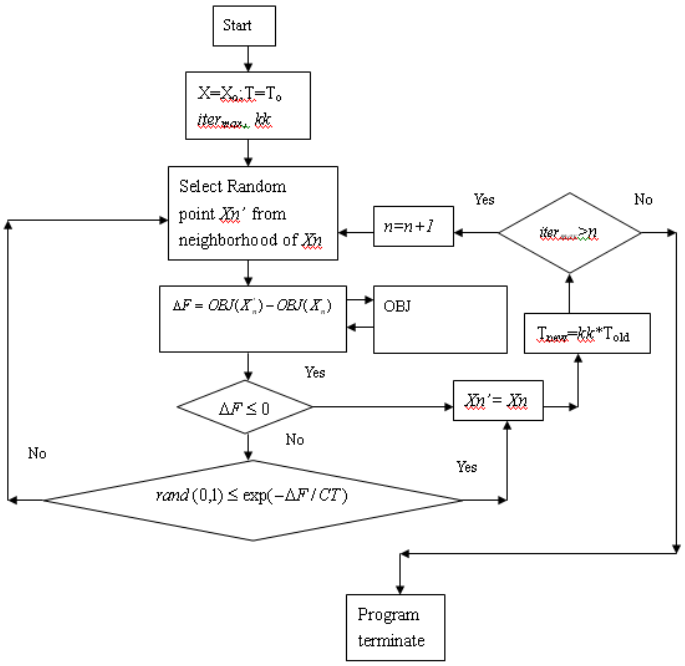

Figure 10 Flow diagram of a SA optimization.

Seven sets of *SA* parameters are tested by varying the values of the *SA* parameters. The simulated results with respect to a pure tone of 250 Hz is summarized and shown in Table 2. As indicated in Table 2, the optimal design data can be obtained from the last set of *SA* parameters at (kk, $iter_{\max}$) = (0.96, 1000). Using the optimal design in a theoretical calculation, the optimal *STL* curves with respect to various *SA* parameters are plotted and depicted in Figures 11. As revealed in Figure 11, the *STL*s are roughly maximized at the desired frequencies.

Table 2 Optimal *STL* for a one-chamber muffler with perforated intruding tubes at various kk and $iter_{\max}$ (targeted tone of 250 Hz).

Item	SA parameters		Results					
	kk	$iter_{max}$						
1	0.90	200	*RT1*	*RT2*	*RT3*	*RT4*	*RT5*	*STL* (dB)
			0.7659	0.3659	0.5989	0.5989	0.59989	44.3
			RT6	*RT7*	*RT8*	*RT9*	*RT10*	
			0.5989	0.005241	0.07654	0.005241	0.07654	
2	0.93	200	*RT1*	*RT2*	*RT3*	*RT4*	*RT5*	*STL* (dB)
			0.8428	0.4428	0.7141	0.7141	0.7141	55.4
			RT6	*RT7*	*RT8*	*RT9*	*RT10*	
			0.7141	0.006249	0.08998	0.006249	0.08998	
3	0.96	200	*RT1*	*RT2*	*RT3*	*RT4*	*RT5*	*STL* (dB)
			0.8664	0.4664	0.7496	0.7496	0.7496	63.7
			RT6	*RT7*	*RT8*	*RT9*	*RT10*	
			0.7496	0.006559	0.09412	0.006559	0.09412	
4	0.99	200	*RT1*	*RT2*	*RT3*	*RT4*	*RT5*	*STL* (dB)
			0.8663	0.4663	0.7495	0.7495	0.7495	63.7
			RT6	*RT7*	*RT8*	*RT9*	*RT10*	
			0.7495	0.006558	0.0941	0.006558	0.0941	
5	0.96	400	*RT1*	*RT2*	*RT3*	*RT4*	*RT5*	*STL* (dB)
			0.8785	0.4785	0.7677	0.7677	0.7677	69.1
			RT6	*RT7*	*RT8*	*RT9*	*RT10*	
			0.7677	0.006718	0.09623	0.006718	0.09623	
6	0.96	800	*RT1*	*RT2*	*RT3*	*RT4*	*RT5*	*STL* (dB)
			0.8829	0.4829	0.7744	0.7744	0.7744	81.4
			RT6	*RT7*	*RT8*	*RT9*	*RT10*	
			0.7744	0.006776	0.09701	0.006776	0.09701	
7	**0.96**	**1000**	*RT1*	*RT2*	*RT3*	*RT4*	*RT5*	*STL* (dB)
			0.8748	**0.4748**	**0.7622**	**0.7622**	**0.7622**	**85.2**
			RT6	*RT7*	*RT8*	*RT9*	*RT10*	
			0.7622	**0.006669**	**0.09559**	**0.006669**	**0.09559**	

7.1.2 Broadband Noise Optimization

By using the above *SA* parameters, the muffler's optimal design data for one-chamber mufflers hybridized with perforated intruding tubes used to minimize the sound power level at the muffler's outlet is summarized in Table 3. As illustrated in Table 3, the resultant sound power levels with respect to three kinds of mufflers have been dramatically reduced from 122.4 dB(A) to 80.1 dB(A). Using this optimal design in a theoretical calculation, the optimal *STL* curves with respect to various *SA* parameters are plotted and compared with the original *SWL* depicted in Figure 12.

Table 3 Optimal *SWL* for a one-chamber muffler with perforated intruding tubes at various *kk* and $iter_{max}$ (broadband noise).

Item	SA parameters		Results					
	kk	itermax						
1	0.90	40	RT1	RT2	RT3	RT4	RT5	SWL_t (dB)
			0.8729	0.4729	0.7593	0.7593	0.7593	98.3
			RT6	RT7	RT8	RT9	RT10	
			0.7593	0.006644	0.09525	0.006644	0.09525	
2	0.93	40	RT1	RT2	RT3	RT4	RT5	SWL_t (dB)
			0.6361	0.2361	0.4041	0.4041	0.4041	93.2
			RT6	RT7	RT8	RT9	RT10	
			0.4041	0.003536	0.05381	0.003536	0.05381	
3	0.96	40	RT1	RT2	RT3	RT4	RT5	SWL_t (dB)
			0.6043	0.2043	0.3564	0.3564	0.3564	90.0
			RT6	RT7	RT8	RT9	RT10	
			0.3564	0.003119	0.04825	0.003119	0.04825	
4	0.99	40	RT1	RT2	RT3	RT4	RT5	SWL_t (dB)
			0.5617	0.1617	0.2926	0.2926	0.2926	92.2
			RT6	RT7	RT8	RT9	RT10	
			0.2926	0.00256	0.0408	0.00256	0.0408	
5	0.96	80	RT1	RT2	RT3	RT4	RT5	SWL_t (dB)
			0.5354	0.1354	0.2531	0.2531	0.2531	88.2
			RT6	RT7	RT8	RT9	RT10	
			0.2531	0.002214	0.03619	0.002214	0.03619	
6	0.96	160	RT1	RT2	RT3	RT4	RT5	SWL_t (dB)
			0.5485	0.1485	0.2727	0.2727	0.2727	86.4
			RT6	RT7	RT8	RT9	RT10	
			0.2727	0.002386	0.03849	0.002386	0.03849	
7	0.96	320	RT1	RT2	RT3	RT4	RT5	SWL_t (dB)
			0.8159	0.4159	0.6738	0.6738	0.6738	84.4
			RT6	RT7	RT8	RT9	RT10	
			0.6738	0.005896	0.08528	0.005896	0.08528	
8	**0.96**	**640**	RT1	RT2	RT3	RT4	RT5	SWL_t (dB)
			0.8101	**0.4101**	**0.6651**	**0.6651**	**0.6651**	**80.1**
			RT6	RT7	RT8	RT9	RT10	
			0.6651	**0.00582**	**0.08426**	**0.00582**	**0.08426**	

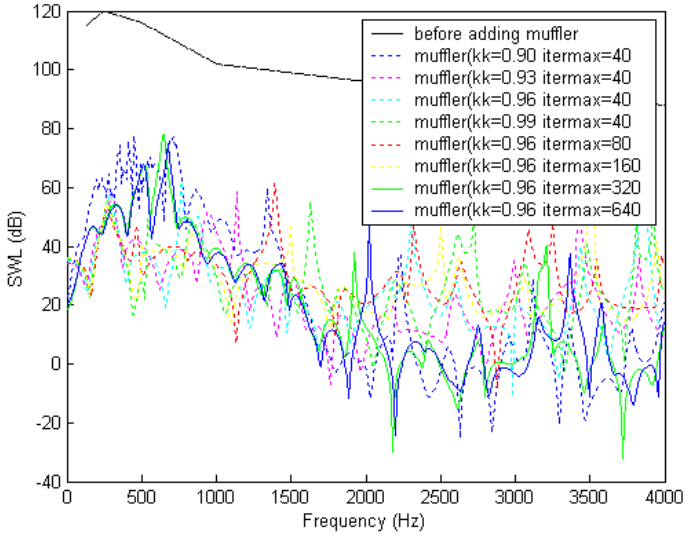

Figure 12 Comparison of the optimal *STL* with respect to original noise level at *kk*=0.96 and $iter_{max}$=640 [broadband noise].

To appreciate the acoustic performance, two kinds of low back-pressure mufflers (a one-chamber simple expansion muffler and a one-chamber muffler hybridized with non-perforated intruding tubes) are optimized. As indicated in Table 4, the resultant SWL with respect to three mufflers (a one-chamber simple expansion muffler, a one-chamber muffler hybridized with perforated intruding tubes, and a one-chamber muffler hybridized with non-perforated intruding tubes) are 94.2 dB, 80.1 dB, and 109.4 dB. Using this optimal design in a theoretical calculation, the optimal *STL* curves with respect to three kinds of optimized mufflers are plotted and compared with original *SWL* shown in Figure 13.

Table 4 Comparison of acoustical performance with respect to three kinds of optimized mufflers within a same space-constrained situation (broadband noise).

Item	Muffler Type	Results					
1	one-chamber simple expansion muffler	$RT1^*$		$RT2^*$		$RT3^*$	SWL_T (dB)
		0.1163		0.2245		0.2245	94.2
2	one-chamber muffler equipped with perforated intruding tubes	$RT1$	$RT2$	$RT3$	$RT4$	$RT5$	SWL_T (dB)
		0.8101	0.4101	0.6651	0.6651	0.6651	80.1
		$RT6$	$RT7$	$RT8$	$RT9$	$RT10$	
		0.6651	0.00582	0.08426	0.00582	0.08426	
3	one-chamber muffler equipped with	$RT1^{**}$		$RT2^{**}$			SWL_T (dB)
		0.2926		0.2926			109.4

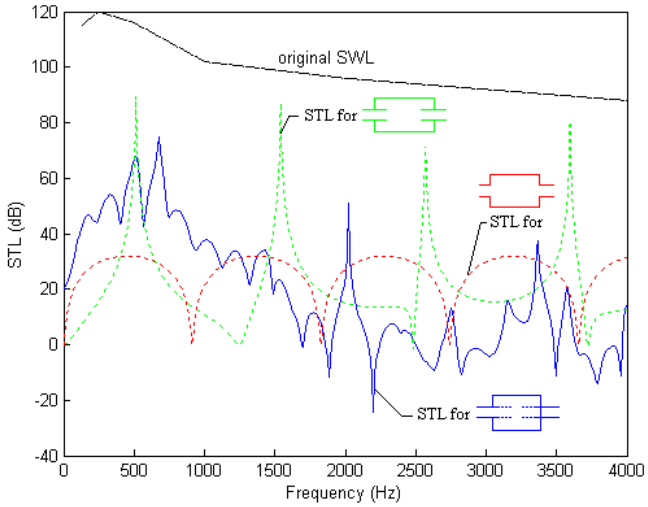

Figure 13 Comparison of the optimal *STL*s of three kinds of mufflers with respect to original noise level [broadband noise].

7.2 Discussion

To achieve a sufficient optimization, the selection of the appropriate *SA* parameters set is essential. As indicated in Table 2, the best *SA* set at the targeted pure tone noise of 250 Hz has been shown. The related *STL* curves with respect to various *SA* parameters are plotted in Figure 11. Figure 11 reveals the predicted maximal value of the *STL* is located at the desired frequency. Therefore, using the *SA* optimization in finding a better design solution is reliable; moreover, in dealing with the broadband noise, the *SA*'s solution shown in Table 3 and Figure 12 can also provide the appropriate and sufficient sound reduction under space-constraint conditions. To investigate the acoustical performance among three kinds of low back-pressure mufflers (a one-chamber simple expansion muffler, a one-chamber muffler hybridized with perforated intruding tubes, and a one-chamber muffler hybridized with non-perforated intruding tubes), the resultant SWL_T is shown in Table 4 and plotted in Figure 13. It is obvious that the one-chamber muffler hybridized with perforated intruding tubes is superior to the other mufflers. As can be observed in Table 4, the overall sound transmission loss of the one-chamber muffler with perforated intruding tubes reaches 43.9 dB. However, the overall sound transmission loss of the one-chamber simple expansion muffler and the one-chamber muffler with non-perforated intruding tubes are 28dB and 12.8 dB.

8. Conclusion

It has been shown that one-chamber mufflers hybridized with perforated intruding tubes can be easily and efficiently optimized within a limited space by using a decoupling technique, a plane wave theory, a four-pole transfer matrix, and a *SA* optimizer. Two kinds of *SA* parameters (kk, $iter_{\max}$) play essential roles in the solution's accuracy during *SA* optimization. As indicated in Figure 11, the tuning ability established by adjusting design parameters of mufflers is reliable.

In addition, the appropriate acoustical performance curve of three kinds of low back-pressure mufflers (a one-chamber simple expansion muffler, a one-chamber muffler hybridized with perforated intruding tubes, and a one-chamber muffler hybridized with non-perforated intruding tubes) has been assessed. As indicated in Table 4, the resultant SWL_T with respect to these mufflers is 94.2 dB, 80.1 dB, and 109.4 dB. As shown in Table 4 and Figure 13, it is quite obvious that the acoustical mechanism using perforated intruding tubes inside the muffler's cavity has the best acoustical performance compared to those with no tubes and non-perforated intruding tubes. Consequently, the approach used for the optimal design of the *STL* proposed in this study is quite efficient in dealing with the industrial venting noise within a space-constrained situation.

9.Reference

1. Magrab, E.B., *Environmental Noise Control*, John Wiley & Sons, New York, 1975.

2. Davis, D.D., Stokes, J.M., Moorse, L., "Theoretical and experimental investigation of mufflers with components on engine muffler design," *NACA Report*, pp. 1192, 1954.

3. Prasad, M.G., "A note on acoustic plane waves in a uniform pipe with mean flow," *Journal of Sound and Vibration*, Vol. 95, No.2, pp. 284-290,1984.

4. Munjal, M.L., *Acoustics of Ducts and Mufflers with Application to Exhaust and Ventilation System Design*, John Wiley & Sons, New York, 1987.

5. Kim, Y.H., Choi, J.W. and Lim, B.D., "Acoustic characteristics of an expansion chamber with constant mass flow and steady temperature gradient (theory and numerical simulation)," *Journal of Vibration and Acoustics*, Vol. 112, pp. 460~467, 1990.

6. Sullivan, J.W. and Crocker, M.J., "Analysis of concentric tube resonators having unpartitioned cavities," *Acous. Soc. Am.*, Vol. 64, pp. 207-215, 1978.

7. Sullivan, J.W., "A method of modeling perforated tube muffler components I: theory," *Acous. Soc. Am.*, Vol. 66, pp. 772-778, 1979.

8. Sullivan, J.W., "A method of modeling perforated tube muffler components I: theory," *Acous. Soc. Am.*, Vol. 66, pp. 779-788, 1979.

9. Thawani, P.T. and Jayaraman, K., "Modeling and applications of straight-through resonators," *Acous. Soc. Am.*, Vol. 73, No. 4, pp. 1387-1389, 1983.

10. Rao, K.N. and Munjal, M.L., "A generalized decoupling method for analyzing perforated element mufflers," Nelson Acoustics Conference, Madison, 1984.

11. Jayaraman, K. and Yam, K., "Decoupling approach to modeling perforated tube muffler component," *Acous. Soc. Am.*, Vol. 69, No. 2, pp. 390-396, 1981.

12. Munjal, M.L., Rao, K.N. and Sahasrabudhe, A. D., "Aeroacoustic analysis of perforated muffler components," *Journal of Sound and*

Vibration, Vol. 114, No. 2, pp. 173-88, 1987.

13. Peat, K.S., "A numerical decoupling analysis of perforated pipe silencer elements," *Journal of Sound and Vibration*, Vol. 123, No. 2, pp. 199-212, 1988.
14. Wang, C.N., "A Numerical Scheme for the Analysis of Perforated Intruding Tube Muffler Components," *Applied Acoustics*, Vol. 44, pp.275-286, 1995.
15. Yeh, L.J., Chang, Y.C., Chiu, M.C. and Lai, G.J., "GA optimization on multi-segments muffler under space constraints," *Applied Acoustics*, Vol. 65, No. 5, pp. 521-543, 2004.
16. Chang, Y.C., Yeh, L.J., Chiu, M.C., Lai, G. J., "Computer aided design on single expansion muffler with extended tube under space constraints," *Tamkang Journal of Science and Engineering*, Vol. 7, No. 3, pp. 171-181, 2004.
17. Chang, Y.C., Yeh, L.J., Chiu, M.C., "GA Optimization on single-chamber muffler hybridized with extended tube under space constraints, "*Archives of Acoustics*, Vol. 29, No. 4, pp.577-596, 2004.
18. Chang, Y.C., Yeh, L.J., Chiu, M.C., "Shape optimization on constrained single-chamber muffler by using GA method and mathematical gradient method**, "***International Journal of Acoustics and Vibration*, Vol.10, No. 1, pp. 17-25, 2005.
19. Munjal, M.L., "Plane wave analysis of side inlet/outlet chamber mufflers with mean flow," *Applied Acoustics*, Vol. 52, No. 2, pp.165-175, 1997.
20. Metropolis, A., Rosenbluth, W., Rosenbluth, M. N., Teller, H., and Teller, E., "Equation of static calculations by fast computing machines," *J. Chem. Phys.*, Vol. 21, No.6, 1087–1092, 1953.
21. Kirkpatrick, S., Gelatt, C. D., and Vecchi, M. P., "Optimization by simulated annealing," *Science*, Vol.220, No.4598, pp. 671–680, 1983.

Acknowledgements

The authors acknowledge the financial support of the National Science Council (NSC 97-2221-E-235 -001, ROC)